

Near-infrared down-conversion luminescence in Yb³⁺ doped self-activated TbZn(B₅O₁₀) phosphor

HAO LI^a, YIXUAN LU^a, CHENXIA LI^{a,*}, DEGANG DENG^{b,*}, KEZHEN RONG^a, XUFENG JING^a, LE WANG^a, SHIQING XU^b

^aCollege of Optical and Electronic Technology, China Jiliang University, Hangzhou, 310018, China

^bCollege of Material Science and Engineering, China Jiliang University, Hangzhou, 310018, China

A series of near-infrared quantum-cutting Tb³⁺-based Tb_{1-x}Zn(B₅O₁₀):xYb³⁺ phosphor was prepared by a high-temperature solid-state method according to rare-earth's self-activation characteristic. The lattice structure and luminescence performances under UV-light's excitation were studied. The conclusion that the doped Yb³⁺ ion only occupies Tb³⁺ ion's site was revealed by XRD patterns. The Tb³⁺ ⁵D₄₋₇F_J characteristic emission spectra and the 974 nm near-infrared light generated by Yb³⁺ ²F_{5/2-2}F_{7/2} emissions were discussed in Tb_{1-x}Zn(B₅O₁₀):xYb³⁺ under 365-nm-UV-light excitation. The cooperative energy transfer mechanism between Tb³⁺ and Yb³⁺ was established by the fluorescence spectra. The above investigations indicate Tb_{1-x}Zn(B₅O₁₀):xYb³⁺ a potential down-converter layer in silicon-based solar cells.

(Received August 26, 2018; accepted June 14, 2019)

Keywords: Phosphor, Tb_{1-x}Zn(B₅O₁₀):xYb³⁺, Cooperative energy transfer

1. Introduction

As for silicon-based solar cells, the thermalization effect of electron-hole pairs caused by absorbing high-energy photons (300–500 nm) is a main mechanism of energy loss. Thus near-infrared (NIR) quantum cutting (QC) phosphors were designed to solve the problem by efficiently converting one ultraviolet-blue photon into two NIR photons which could be absorbed by Si ($E > 1.12$ eV, $\lambda_{\text{abs}} < 1100$ nm) afterwards [1-3,6,7,9]. These few years, therefore, the NIR QC materials had caused widespread concern in the research area of solar cells [3].

Rare-earth elements were widely used to synthesize QC phosphors. Specifically, the Yb³⁺ ion is an ideal material for down-conversion process as both an activator and an acceptor. Its NIR emission near 980 nm can match well with the band gap of crystalline Si [5,10]. Besides, rare earths were used as sensitizers, such as Pr³⁺, Gd³⁺, Tb³⁺ ions. They transfer energy to Yb³⁺ through cooperative energy transfer (ET) mechanism. However, the conditions for effective excitation of Pr³⁺ and Gd³⁺ are excited by vacuum ultraviolet (VUV) photons ($\lambda = 125-215$ nm). Since the energy of ⁵D₄ level matches nearly twice as the Yb³⁺ ²F_{5/2} level, thus, made Tb³⁺ a promising sensitizer. Therefore, the blue photons generated by one Tb³⁺ excitation can cause Yb³⁺ to generate two 980 nm near-infrared photons. However, to our knowledge, concentration quenching is widespread in the rare earth-doped phosphors. Hence, rare earth self-activated materials were designed to release this

phenomenon, which rare earths were doped as substance.

The ET from Tb³⁺ to Yb³⁺ through cooperative down-conversion has been studied in various materials including borates [6,19], phosphates, oxides [3,7]. Among them, borates might be a scientific host community for down-conversion phosphors, because of their stable thermochemical properties, low synthetic temperature and wide range of applications, etc.

A novel Tb³⁺-based borate down-conversion QC phosphors Tb_{1-x}Zn(B₅O₁₀):xYb³⁺ was prepared by a solid-state method in this article. The crystal structure and photoluminescence (PL) properties of Tb_{1-x}Zn(B₅O₁₀):xYb³⁺ phosphor were systematically investigated in detail. The energy transfer mechanism has been systematically explained by the emission, excitation, diffuse reflection and fluorescence decay spectra. All the conclusions indicated that Tb_{1-x}Zn(B₅O₁₀):xYb³⁺ has great potential in silicon-based solar cells as a down-converter layer [24,25].

2. Experimental section

2.1. Sample preparation

A high-temperature solid-state method was taken to prepare the sample powder. Raw materials for synthesizing Tb_{1-x}Zn(B₅O₁₀):xYb³⁺ (0 ≤ x ≤ 0.25) samples include Tb₄O₇ (A.R.), ZnO (A.R.), H₃BO₃ (A.R.) and Yb₂O₃ (A.R.). They are needed to be well-weighted in

the light of the stoichiometric ratio. After the reagents were thoroughly mixed and ground in an agate mortar, they would be placed in an alumina crucible with anhydrous as a medium, which then would be heated in a tube-type program resistance furnace. A Sintering environment would be set at 950°C for 2 hours with a 7 °C per minute heating rate for the evenly mixed powders within a reducing atmosphere (5% H₂/ 95% N₂). The obtained phosphor samples cooled to room temperature would be ground into powder to carry out future measurements.

2.2. Characterization

X-ray diffraction (XRD) was employed to test phase purity with the parameter of Bruker Axs D2 PHASER diffractometer. Cu $k\alpha=0.15406$ nm, 2θ range of 10° to 80°, 30 kV accelerating voltage and 10 mA current. For Energy-dispersive spectrometer (EDS), a field-emission scanning electron microscope (FE-SEM, S-4800, Hitachi, Japan) was adopted as the testing instrument, with its Interplanar crystal spacing investigated by a transmission electron microscope (TEM), the type of which being FE-SEM, S-4800, Hitachi Japan. For the quantity of Excitation and emission spectra, a Spectrometer was used as the tool of examination, which falls under the type of PL-3-211, HORIBA JOBIN YVON America, compounded with a 450 W xenon lamp as light source of excitation. For Diffuse reflectance spectra, they were tested by a UV-Visible spectrometer, the type of which being UV-3600, Shimadzu Japan, and a white powder

BaSO₄ is considered as a reference. The above testings were carried out with a controlled room temperature.

3. Results and discussions

3.1. Phase identification and crystal structure

The Tb_{1-x}Zn(B₅O₁₀):xYb³⁺ (0≤x≤0.25) phosphor sample powder's XRD patterns and the TbZn(B₅O₁₀) (JCPDS 86-1886) standard data for comparison are shown in Fig. 1 (a). Any byproducts (JCPDS) in the database cannot indexed to the sample patterns obtained. However, by comparing with the JCPDS 86-1886 standard card, all diffraction peaks of sample were found to be well indexed, only except for a small drift towards the higher 2θ angle (seen in Fig. 1 (b)). The result clearly showed that the prepared Tb_{1-x}Zn(B₅O₁₀):xYb³⁺ phosphor can be identified as an isostructural crystal of TbZn(B₅O₁₀). Moreover, the higher angular small drift results from the substitution of larger Tb³⁺ ions by smaller Yb³⁺ ions.

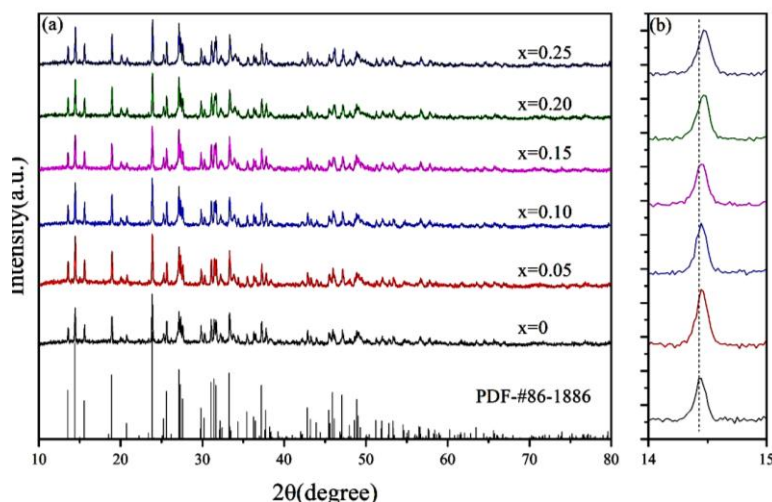


Fig. 1 (a) XRD patterns of the Tb_{1-x}Zn(B₅O₁₀):xYb³⁺ (0≤x≤0.25) samples and the standard data of TbZn(B₅O₁₀) (JCPDS 86-1886) as a reference. (b) Magnified XRD patterns falls in the range between 14° and 15°

In order to acquire the detailed crystal structure parameters, a computer software Topas was applied to refine the Rietveld structure of the Tb_{1-x}Zn(B₅O₁₀):xYb³⁺ (0≤x≤0.25) sample's XRD patterns, as Fig. 2 (a)-(f) show. The structure data of TbZn(B₅O₁₀) were used as an initial model for crystal structure of them that bears a certain

similarity. Table 1 (a)-(f) show the fractional atomic coordinates, occupancy and reliability parameters. Since Yb³⁺ and Tb³⁺ both belong to the lanthanide and have similar ionic radius, Tb³⁺ can be replaced by Yb³⁺ without changing the lattice structure of the matrix. The obtained Tb_{1-x}Zn(B₅O₁₀):xYb³⁺ sample belongs to the

monoclinic system, and its space group belongs to $\text{P121/n}(14)$. The parameters of unit cell volume obtained by Rietveld structure refinement, were shown in Fig. 3. With the augment of Yb^{3+} doping concentration, the cell

volume of $\text{Tb}_{1-x}\text{Zn}(\text{B}_5\text{O}_{10}):x\text{Yb}^{3+}$ decreases, which proved that Yb^{3+} has replaced the host lattice of Tb^{3+} into the matrix.

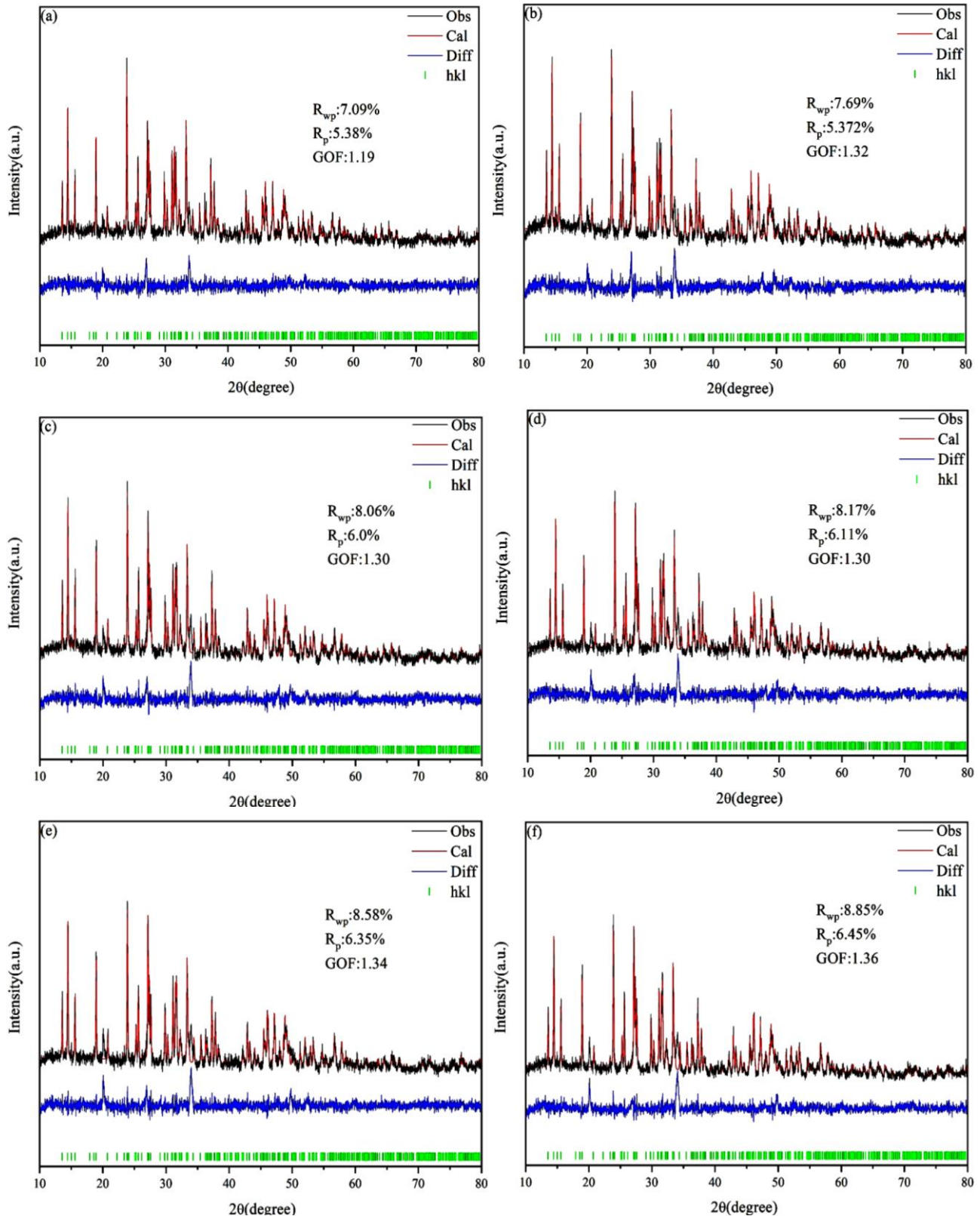


Fig. 2. (a)-(f) Rietveld refinement XRD patterns of $\text{Tb}_{1-x}\text{Zn}(\text{B}_5\text{O}_{10}):x\text{Yb}^{3+}$ ($0 \leq x \leq 0.25$) by TOPAS package

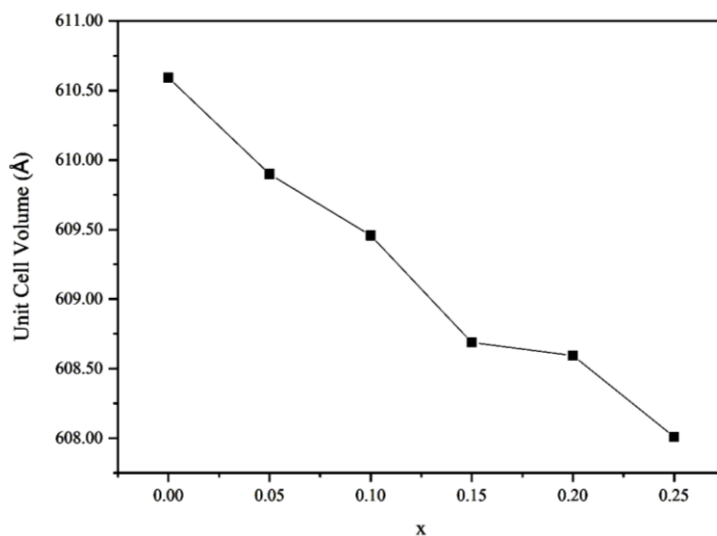


Fig. 3. Unit cell volume of the $Tb_{1-x}Zn(B_5O_{10}):xYb^{3+}$ ($0 \leq x \leq 0.25$)

Table 1(a). The refinement data and fractional atomic coordinates of $Tb_{1-x}Zn(B_5O_{10}):xYb^{3+}$ ($x=0$)

Space group: P121/n1 (14) (monoclinic)					
Cell parameter			Reliability Factors		
Crystal Density (g/cm^3)= 4.769			Rexp(%)=5.94		
Z=4			Rwp(%)=7.09		
$a = 8.5731123 \text{ \AA}$			Rp(%)=5.38		
$b = 7.6031647 \text{ \AA}$			GOF= 1.19		
$c = 9.3849468 \text{ \AA}$					
$\beta = 93.50522 \text{ \AA}^3$					
$V = 610.59256 \text{ \AA}^3$					
Atom	x	y	z	Occupancy	Beq
Zn1/Mn1	0.6068	0.40764	0.12468	1	0
Tb1	0.18548	0.18376	0.23885	1	0
B1	0.87666	0.60762	0.27263	1	1.9
B2	0.46432	0.29889	0.37745	1	-1.485
B3	0.71396	0.50974	0.41949	1	-5.403
B4	0.89563	0.6124	-0.02734	1	2.305
B5	0.96148	0.34825	0.4047	1	-0.2256
O1	0.02122	0.68397	0.23616	1	0
O2	0.81366	0.5287	0.1178	1	0
O3	0.99024	0.40226	0.29944	1	0
O4	0.79291	0.6476	0.37077	1	0
O5	0.59972	0.47117	0.33347	1	0
O6	0.33182	0.40328	0.42493	1	0
O7	0.55119	0.22259	0.5249	1	0
O8	0.82223	0.36404	0.48668	1	0
O9	0.49898	0.63348	0.0661	1	0
O10	0.25093	0.46437	0.12017	1	0

Table 1 (b). The refinement data and fractional atomic coordinates of Tb_{1-x}Zn(B₅O₁₀):xYb³⁺ (x=0.05)

Space group: P121/n1 (14) (monoclinic)					
Cell parameter			Reliability Factors		
Crystal Density (g/cm ³)= 4.774			Rexp(%)=5.85		
Z=4			Rwp(%)=7.69		
a = 8.5670288 Å			Rp(%)=5.72		
b = 7.6027498 Å			GOF= 1.32		
c = 9.3817657 Å					
β= 93.53501 Å ³					
V = 609.89966 Å ³					
Atom	x	y	z	Occupancy	Beq
Zn1/Mn1	0.60643	0.41078	0.12743	1	0
Tb1	0.18478	0.18273	0.24147	1	0
B1	0.86983	0.59052	0.23538	1	-0.04776
B2	0.44432	0.3054	0.3636	1	-0.9407
B3	0.68667	0.50987	0.44901	1	1.54
B4	0.88843	0.62406	-0.02558	1	0.2986
B5	0.97461	0.34342	0.43046	1	-4.57
O1	0.02747	0.70265	0.22051	1	0
O2	0.80481	0.52401	0.10312	1	0
O3	0.99058	0.40195	0.30117	1	0
O4	0.80505	0.63123	0.3643	1	0
O5	0.59789	0.47259	0.32645	1	0
O6	0.31983	0.39325	0.42777	1	0
O7	0.54865	0.2295	0.52623	1	0
O8	0.82323	0.36436	0.49122	1	0
O9	0.48511	0.63214	0.07202	1	0
O10	0.25395	0.46272	0.13824	1	0

Table 1 (c). The refinement data and fractional atomic coordinates of Tb_{1-x}Zn(B₅O₁₀):xYb³⁺ (x=0.01)

Space group: P121/n1 (14) (monoclinic)					
Cell parameter			Reliability Factors		
Crystal Density (g/cm ³)= 4.778			Rexp(%)=6.18		
Z=4			Rwp(%)=8.06		
a = 8.5625024 Å			Rp(%)=6.00		
b = 7.6028885 Å			GOF= 1.30		
c = 9.3799809 Å					
β= 93.55802 Å ³					
V = 609.45741 Å ³					
Atom	x	y	z	Occupancy	Beq
Zn1/Mn1	0.6069	0.4087	0.12729	1	0
Tb1	0.18494	0.18329	0.23964	1	0
B1	0.87978	0.59575	0.25182	1	1.583
B2	0.46248	0.27873	0.3759	1	-2.641
B3	0.70378	0.51119	0.45353	1	-6.264
B4	0.87456	0.61548	-0.01366	1	-4.823
B5	0.97428	0.34148	0.4249	1	-3.9
O1	0.0335	0.68643	0.23953	1	0
O2	0.79713	0.51846	0.11185	1	0
O3	0.99009	0.40724	0.2992	1	0
O4	0.78884	0.63585	0.3654	1	0
O5	0.59143	0.47748	0.332	1	0
O6	0.33293	0.37827	0.41871	1	0

Space group: P121/n1 (14)(monoclinic)					
O7	0.55149	0.22982	0.51878	1	0
O8	0.81678	0.36991	0.48533	1	0
O9	0.48289	0.63118	0.07139	1	0
O10	0.25094	0.45936	0.12742	1	0

Table 1 (d). The refinement data and fractional atomic coordinates of $Tb_{1-x}Zn(B_5O_{10}):xYb^{3+}(x=0.15)$

Space group: P121/n1 (14)(monoclinic)					
Cell parameter			Reliability Factors		
Crystal Density (g/cm ³)= 4.784			Rexp(%)=6.30		
Z=4			Rwp(%)=8.17		
$a = 8.5570152 \text{ \AA}$			Rp(%)=6.11		
$b = 7.6020177 \text{ \AA}$			GOF= 1.30		
$c = 9.3755403 \text{ \AA}$					
$\beta = 93.58836 \text{ \AA}^3$					
$V = 608.68864 \text{ \AA}^3$					
Atom	x	y	z	Occupancy	Beq
Zn1/Mn1	0.60626	0.40659	0.12836	1	0
Tb1	0.1845	0.18357	0.24057	1	0
B1	0.86919	0.59015	0.25315	1	-2.657
B2	0.48156	0.25529	0.3857	1	-3.252
B3	0.71464	0.50729	0.45249	1	-6.116
B4	0.88379	0.61205	-0.01417	1	-6.579
B5	0.96337	0.37215	0.43641	1	-5.783
O1	0.03265	0.69229	0.24236	1	0
O2	0.80252	0.52987	0.11176	1	0
O3	0.9801	0.40359	0.29776	1	0
O4	0.79292	0.63109	0.36939	1	0
O5	0.59659	0.47249	0.33252	1	0
O6	0.34267	0.37588	0.42483	1	0
O7	0.54281	0.22741	0.52973	1	0
O8	0.81903	0.36918	0.49272	1	0
O9	0.49592	0.63864	0.07254	1	0
O10	0.26277	0.45651	0.12423	1	0

Table 1 (e). The refinement data and fractional atomic coordinates of $Tb_{1-x}Zn(B_5O_{10}):xYb^{3+}(x=0.2)$

Space group: P121/n1 (14)(monoclinic)					
Cell parameter			Reliability Factors		
Crystal Density (g/cm ³)= 4.784			Rexp(%)=6.40		
Z=4			Rwp(%)=8.58		
$a = 8.5541286 \text{ \AA}$			Rp(%)=6.35		
$b = 7.6030778 \text{ \AA}$			GOF= 1.34		
$c = 9.3762225 \text{ \AA}$					
$\beta = 93.61533 \text{ \AA}^3$					
$V = 608.59441 \text{ \AA}^3$					
Atom	x	y	z	Occupancy	Beq
Zn1/Mn1	0.60681	0.40966	0.12527	1	0
Tb1	0.18654	0.18398	0.23945	1	0
B1	0.86903	0.60889	0.30142	1	-1.226
B2	0.47978	0.25468	0.3791	1	-4.856
B3	0.67551	0.49184	0.44529	1	-3.236
B4	0.88177	0.60589	-0.03176	1	-0.9638
B5	0.95563	0.35469	0.42256	1	-2.578
O1	0.02862	0.68339	0.2418	1	0

Space group: P121/n1 (14)(monoclinic)					
O2	0.81216	0.53924	0.12476	1	0
O3	0.99934	0.40899	0.30128	1	0
O4	0.75821	0.60617	0.37543	1	0
O5	0.59694	0.4599	0.32259	1	0
O6	0.33256	0.36639	0.41411	1	0
O7	0.55946	0.23273	0.52182	1	0
O8	0.81968	0.37852	0.48528	1	0
O9	0.49367	0.6405	0.06934	1	0
O10	0.26269	0.47341	0.12617	1	0

Table 1 (f). The refinement data and fractional atomic coordinates of Tb_{1-x}Zn(B₅O₁₀):xYb³⁺ (x=0.25)

Space group: P121/n1 (14)(monoclinic)					
Cell parameter			Reliability Factors		
Crystal Density (g/cm ³)= 4.789			Rexp(%)=6.52		
Z=4			Rwp(%)=8.85		
a = 8.5487367 Å			Rp(%)=6.45		
b = 7.6028966 Å			GOF= 1.36		
c = 9.3736394 Å					
β= 93.64258 Å ³					
V = 608.01041 Å ³					
Atom	x	y	z	Occupancy	Beq
Zn1/Mn1	0.60926	0.41003	0.12625	1	0
Tb1	0.185	0.18324	0.23985	1	0
B1	0.90646	0.6235	0.35604	1	3.098
B2	0.47896	0.25762	0.38603	1	-4.25
B3	0.67008	0.48664	0.45378	1	-4.397
B4	0.8923	0.60519	-0.01828	1	-0.9263
B5	0.95078	0.35576	0.41036	1	-3.966
O1	0.03553	0.69431	0.24082	1	0
O2	0.81858	0.54666	0.14129	1	0
O3	0.99707	0.40404	0.30259	1	0
O4	0.75551	0.6171	0.36441	1	0
O5	0.58768	0.4702	0.32882	1	0
O6	0.33356	0.35809	0.41814	1	0
O7	0.56665	0.23145	0.53422	1	0
O8	0.8241	0.38016	0.47634	1	0
O9	0.49806	0.63391	0.0654	1	0
O10	0.25652	0.46335	0.11537	1	0

The crystal structure of Tb_{1-x}Zn(B₅O₁₀):xYb³⁺ unit cell along the b-axis direction is shown in Fig. 4 (a). The coordination environment models of Zn and Tb/Yb sites in the Tb_{1-x}Zn(B₅O₁₀):xYb³⁺ crystal structure could be presented based on the result of ICSD-404539 and Rietveld refinement, as are shown in Fig. 4 (b) and (c).

Among them, Tb³⁺/Yb³⁺ is in a 10-fold coordination environment composed of 10 O and Zn²⁺ is in a 6-fold coordination environment of a distorted octahedron composed of 6 O. Since Tb³⁺ has only one kind of position in the crystal structure of Tb_{1-x}Zn(B₅O₁₀):xYb³⁺, there is only one type of Yb³⁺ substitution.

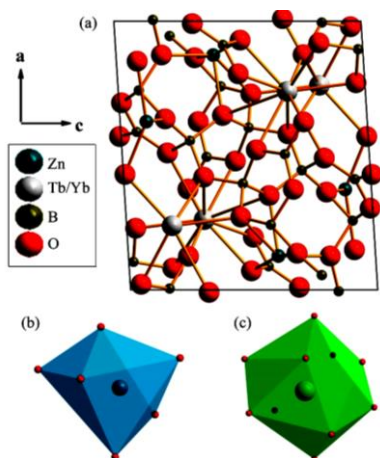


Fig. 4. (a) Schematic structure of $Tb_{1-x}Zn(B_5O_{10}):xYb^{3+}$ (black solid lines denote the unit cell), (b) and (c) were the coordination environment of Zn and Tb/Yb sites in $TbZn_{1-x}(BO_2)_5:xYb^{3+}$, individually.

Fig. 5 (a) shows the energy dispersive spectrum of $Tb_{1-x}Zn(B_5O_{10}):xYb^{3+}$, which indicates the presence of elements B, O, Yb, Tb and Zn in the crystal. In addition, the trace amounts of C and Al may be caused by conductive tapes and the Al-substrate required for SEM testing. The TEM image of $Tb_{1-x}Zn(B_5O_{10}):xYb^{3+}$ was shown in Fig. 5 (b). Based on the crystal lattice stripe, the interplanar crystal spacing of (1 0 1) crystal orientation can be calculated as 0.610 nm.

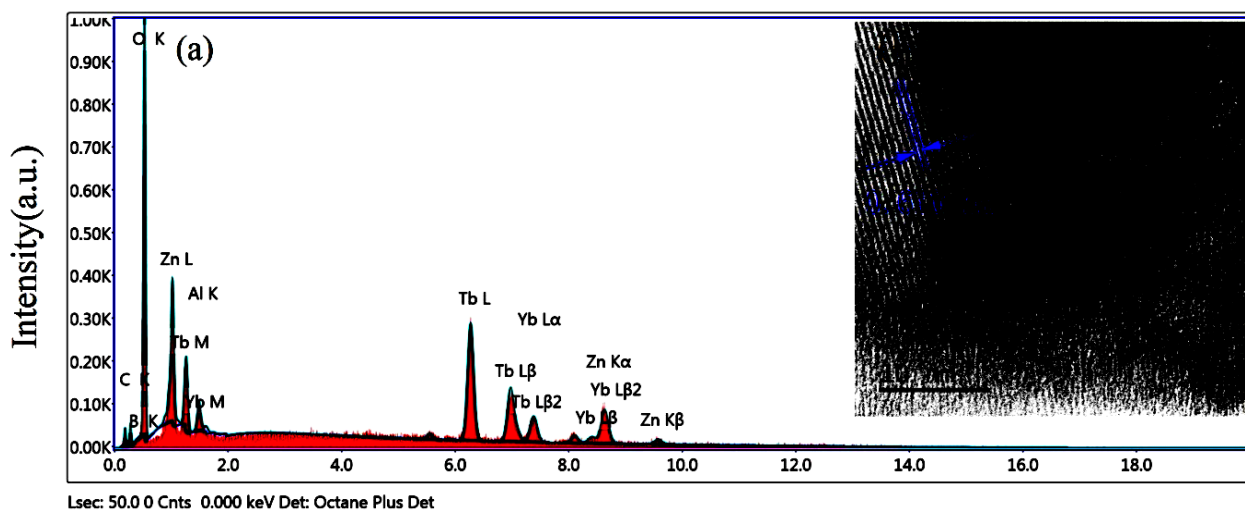


Fig. 5. (a) EDS and (b) SEM image of $Tb_{1-x}Zn(B_5O_{10}):xYb^{3+}$

3.2. Diffuse reflection spectra

The diffuse reflection spectrum of the $Tb_{1-x}Zn(B_5O_{10}):xYb^{3+}$ in the range of 200 to 800 nm is presented in Fig. 6 (a). The results show that the phosphor has a high reflectance in the visible range.

The absorption peak within the scope of 200 nm to 400 nm is the characteristic absorption peak of the Tb^{3+} -based $TbZn(B_5O_{10})$ phosphor.

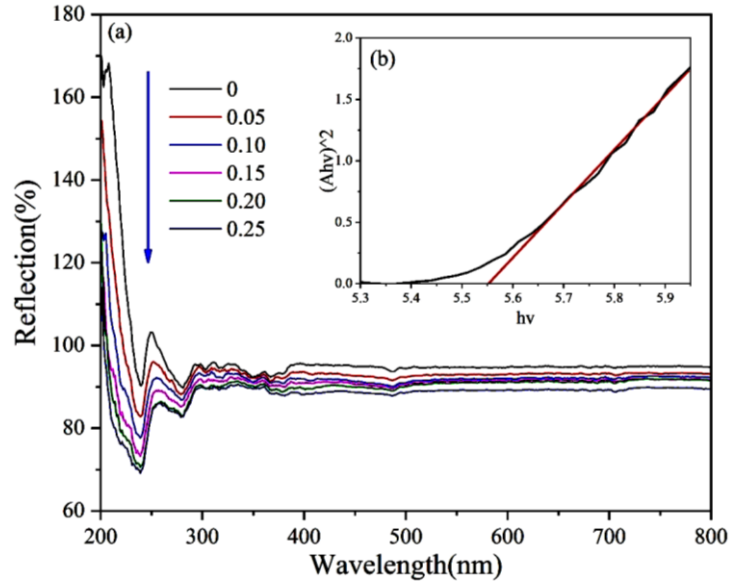


Fig. 6. (a) Diffuse reflection spectrum of the $Tb_{1-x}Zn(B_5O_{10}):xYb^{3+}$ ($0 \leq x \leq 0.25$); (b) absorption spectra of $TbZn(B_5O_{10})$ as calculated by the Kubelka-Munk formula

The spin-allowed and spin-forbidden $f \rightarrow d$ transitions of Tb^{3+} are responsible for the absorption peaks at 239 nm and 280 nm. As the Yb^{3+} ion doping concentration continues to increase, the absorption intensity enhanced correspondingly with no peak shape changes. Compared with the diffuse reflection spectrum of $TbZn(B_5O_{10})$, the absorption intensity in the range of 200-230 nm is significantly enhanced as the Yb^{3+} doping concentration increased, which might due to the $Yb^{3+}-O^{2-}$ charge transfer (CT) transition. The energy gap can be calculated by the following equation [20]:

$$[F(R_{\infty})hv]^n = A(hv - E_g) \quad (1)$$

where hv refers to the photon energy, A is considered as a proportional constant, E_g indicates the value of the bandgap energy, $n=2$ in the case of direct transition while $n=1/2$ is for an indirect transition, and the Kubelka-Munk function $F(R_{\infty})$ is defined as followed [21]:

$$F(R_{\infty}) = (1 - R)^2 / 2R = K / S \quad (2)$$

where R , K and S represent the reflection, the absorption and the scattering coefficient respectively. Using a linear extrapolation of $[F(R_{\infty})hv]^2 = 0$, E_g value could be calculated to be approximately 5.552 eV (see Fig. 6 (b)).

3.3. Photoluminescence properties

The emission spectra of $Tb_{1-x}Zn(B_5O_{10}):xYb^{3+}$ ($0 \leq x \leq 0.25$) in visible light range under the 364 nm excitation is shown in Fig. 7 (a). The emission peaks at

489, 544, 589 and 624 nm were generated by typical transitions $^5D_4 \rightarrow ^7F_J$ ($J=6,5,4,3$) of Tb^{3+} . Among them, the peak position at 544 nm is the main luminescence peak position. And the relative intensity at 544 nm was shown in Fig. 7 (b). As the Yb^{3+} doping concentration increases, the emission intensity at 544 nm is continuously weakened. As anticipated, the $TbZn(B_5O_{10}):Yb$ phosphor did not emit light in the near-infrared spectral range. The NIR emission at 974 nm and the three peaks at 935, 1011, and 1036 nm occur only after Yb^{3+} doping. Since Tb^{3+} exhibits no NIR PL in this spectral region, all near-infrared luminescence is generated by the radiation attenuation from $^2F_{2/5}$ of Yb^{3+} to four different stark levels of the $^2F_{2/7}$ ground state. However, as the Yb^{3+} concentration increased, the NIR emission intensity of Yb^{3+} was gradually enhanced before the doping concentration reaches $x=0.1$. After that, the concentration quenching phenomenon occurs and the NIR luminescence intensity begins to weaken continuously (see in Fig. 7 (c)). This is due to the energy transfer between the sensitizer Tb^{3+} and the activator Yb^{3+} . The energy transfer efficiency (η_T) between Tb^{3+} and Yb^{3+} can be calculated by the following equation [21]:

$$\eta_T = 1 - \frac{I_{s0}}{I_s} \quad (3)$$

where I_{s0} and I_s represent the sensitizers' (Tb^{3+}) emission intensity with activators (Yb^{3+}) absented and presented, respectively. The η_T of $Tb_{1-x}Zn(B_5O_{10}):xYb^{3+}$ was calculated (see Fig. 7 (e)), where it was found that η_T went up as the content of Yb^{3+} increased. And before the concentration quenching occurs, the energy transfer efficiency (η_T) could reach ~12.45%. The energy transfer critical distance (R_c) proposed by Blasse, can also explain

the above phenomenon. R_c can be calculated by using the equation as follows [11]:

$$R_c = 2 \left[\frac{3V}{2\pi\chi_c Z} \right]^{1/3} \quad (4)$$

where V is the cell volume (in \AA^3); χ_c represents the critical concentration; and Z is the number of chemical formulas in the unit cell. In the structure of $\text{TbZn}(\text{B}_5\text{O}_{10})$, by substituting $V = 611.86 \text{\AA}^3$, $Z = 4$, $\chi_c = 0.1$ into the above equation, R_c is calculated to be 18.01\AA , which is far greater than 5\AA . This manifests that the possibility of $\text{ET}_{\text{Tb-Yb}}$ through exchange interaction mechanism is small. Under these circumstances, the energy transfer mechanism could be illustrated by the electric multipole interactions, which include electric dipole-electric dipole,

electric dipole-quadrupoles, and electric quadrupoles-electric quadrupoles. The emission intensity of each activator ion is indicated as followed [22]:

$$I/x = k \left[1 + \beta(x)^{\theta/3} \right]^{-1} \quad (5)$$

where I is the emission intensity; x is the concentration of activators; for a given host-crystal, k and β are both constants under excitations of identical wavelength; $\theta = 3$ represents the energy transfer between the nearest-neighbor ions. However, θ is 6, 8 or 10 correlating to an electric dipole-electric dipole, an electric dipole-electric quadrupoles and an electric quadrupoles-electric quadrupoles interaction respectively.

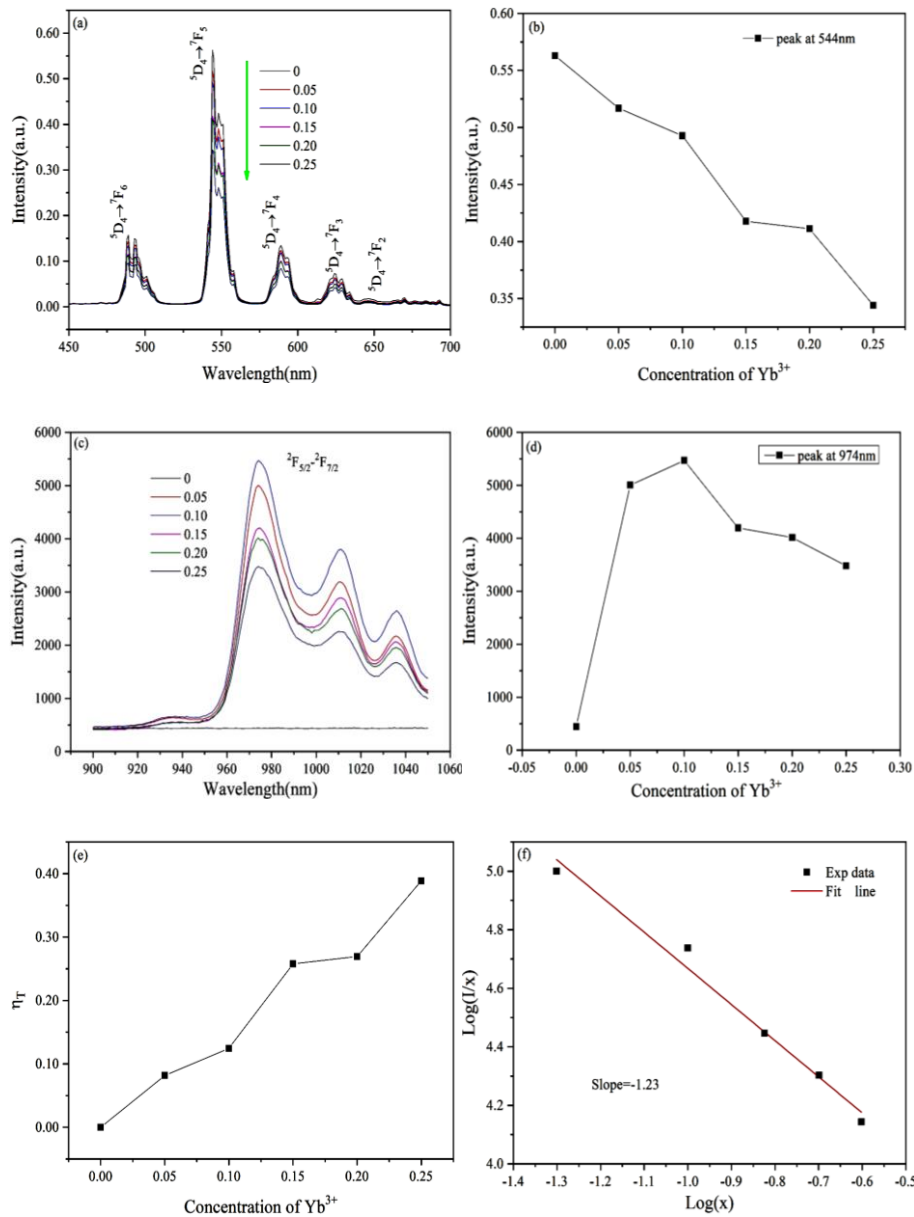


Fig. 7. (a) Emission spectra of $\text{Tb}_{1-x}\text{Zn}(\text{B}_5\text{O}_{10}):x\text{Yb}^{3+}$ ($0 \leq x \leq 0.25$) in visible region under the excitation of 364 nm. (b) Relative intensity at 544 nm. (c) Emission spectra of $\text{Tb}_{1-x}\text{Zn}(\text{B}_5\text{O}_{10}):x\text{Yb}^{3+}$ ($0 \leq x \leq 0.25$) in Near-infrared region. (d) Relative intensity at 974 nm. (e) Transmission efficiency of $\text{Tb}_{1-x}\text{Zn}(\text{B}_5\text{O}_{10}):x\text{Yb}^{3+}$ were calculated. (f) The correlation between $\log(I/x)$ and $\log(x)$ of $\text{Tb}_{1-x}\text{Zn}(\text{B}_5\text{O}_{10}):x\text{Yb}^{3+}$ ($0 \leq x \leq 0.25$).

Fig. 7 (f) shows the linear relationship curve between $\log(I/x)$ and $\log(x)$, which slope is -1.23. Substituting the slope into the above equation gives θ of approximately 3.69, approaching 3, revealing that the phenomenon of concentration quenching of Tb_{1-x}Zn(B₅O₁₀):xYb³⁺ (0 ≤ x ≤ 0.25) phosphor, which derives from the energy transfer between nearest-neighbor ions.

The excitation spectra of Tb_{1-x}Zn(B₅O₁₀):xYb³⁺ (x=0.1) speculated at 544 and 974 nm are shown in Fig. 8. The result shows that the two excitation spectra overlap within the 330-450 nm range. It is reasonable to speculate that this energy transfer exists between Tb³⁺

and Yb³⁺ and has an efficient energy transfer efficiency owing to an extensive overlap. Speculated at 544 nm, the excitation peak at 280 nm can be generated by the Tb³⁺ spin-forbidden f-d transition, and the sharp excitation peaks in the range of 300-500 nm can be generated by the f-f transition of Tb³⁺. Monitored at 974nm, the excitation peaks at 350, 367 and 376 nm correspond to the three split levels transition from Yb³⁺ ²F_{7/2} energy level to ²F_{2/5} energy level respectively.

The NIR quantum cutting through a cooperative energy transferring in Tb_{1-x}Zn(B₅O₁₀):xYb³⁺ is shown in Fig. 9.

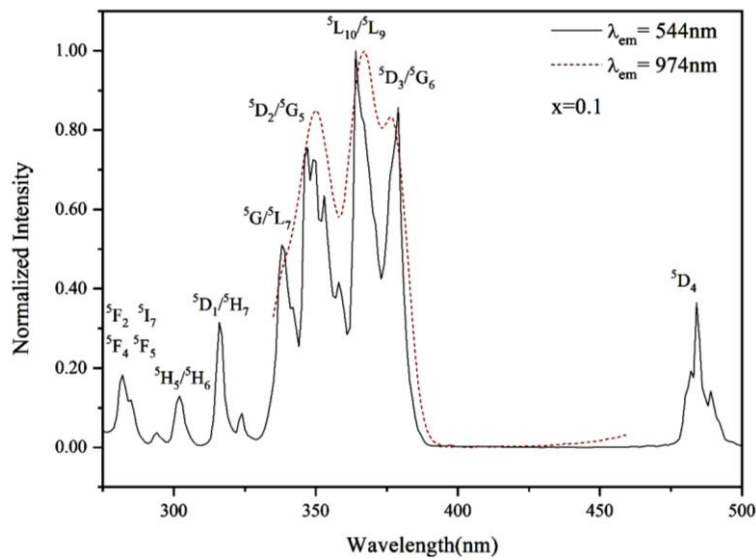


Fig. 8. Excitation spectra of Tb_{1-x}Zn(B₅O₁₀):xYb³⁺ (x=0.1) monitored at 544 nm and 974 nm

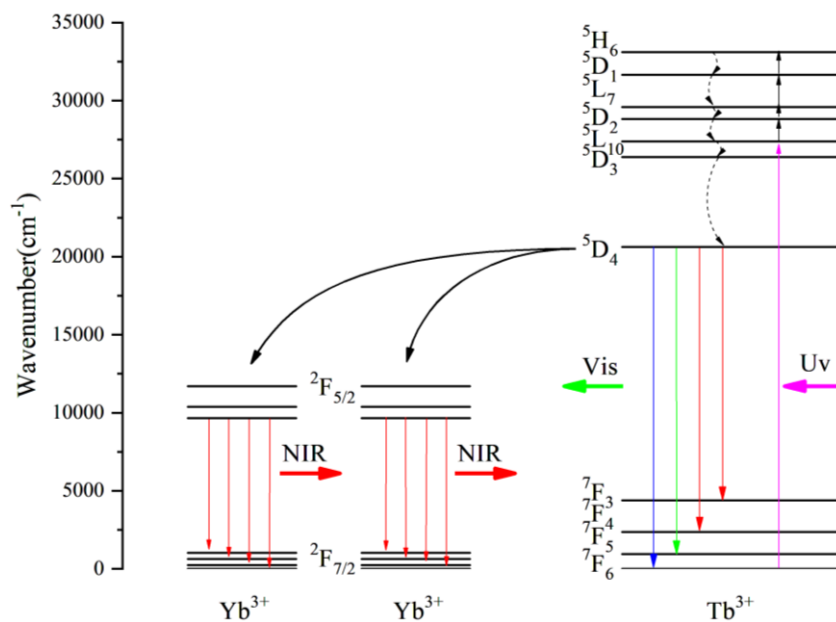


Fig. 9. Schematic of the energy level system demonstrating cooperative energy transfer in the Tb_{1-x}Zn(B₅O₁₀):xYb³⁺ phosphor

The Tb^{3+} ions are excited up to $4f^75d^1$ state by absorbing UV photons (under the excitation of 367 nm), then relaxes to 5D_4 levels non-radiatively. Subsequently, radiative transitions from 5D_4 to various 7F_J ($J = 3, 4, 5, 6$) levels and the cooperative $Tb^{3+}(^5D_4) \rightarrow ^2Yb^{3+}(^2F_{5/2})$ transfer were generated. Hence, the energy excited by one Tb^{3+} ion can be transferred to two different Yb^{3+} ions. Its down-conversion process can be expressed as $^5D_4 \rightarrow ^2F_{5/2} + ^2F_{5/2}$.

4. Conclusions

A new rare-earth based self-excited borate $Tb_{1-x}Zn(B_5O_{10}):xYb^{3+}$ series phosphor was successfully prepared by a high-temperature solid-state method. Its lattice structure and luminescence performances were systematically studied. The main conclusions can be drawn that the doped Yb^{3+} ions only occupy Tb^{3+} ions' sites in the $Tb_{1-x}Zn(B_5O_{10}):xYb^{3+}$ lattice and can generate both 974 nm NIR emission generated by Yb^{3+} ions, and 544 nm green light generated by Tb^{3+} ions under 367 nm excitation. The critical distance calculated by concentration quenching theory is 18.01\AA . The cooperative energy transfer mechanism between nearest-neighbor Tb^{3+} ions and Yb^{3+} ions could be proved by studying the overlap between the excitation spectrum, emission spectrum as well as the fluorescence lifetime decay curve. All the conclusions indicated that $Tb_{1-x}Zn(B_5O_{10}):xYb^{3+}$ is a potential down-converter layer in silicon-based solar cells.

Acknowledgements

This research was supported by the National Key R&D Plan (No. 2017YFB0403100 and 2017YFB0403105); the National Natural Science Foundation of China (No. 61575182); and the Preeminence Youth Science Funds of Zhejiang Province (No. LR19F050001).

References

- [1] Xiaoyong Huang, Qinyuan Zhang, Journal of Applied Physics **105**, 663 (2009).
- [2] Y. P. Peng, W. Lu, P. Ren, Y. Ni, Y. Wang, L. Zhang, S. Ruan, Photonics Research **6**(10), 943 (2018).
- [3] Li Li, Xiantao Wei, Yonghu Chen, Journal of Rare Earths **30**, 197 (2012).
- [4] Y. Jia, Y. Shan, L. Wu, X. Dai, D. Fan, Y. Xiang, Photonics Research **6**(11) 1040 (2018).
- [5] Jiayue Sun, Yining Sun, Junhui Zeng, Jicheng Zhu, Haiyan Du, Advanced Materials Research **683**, 172 (2013).
- [6] A. A. Lyapin, S. V. Gushchin, A. S. Ermakov, S. V. Kuznetsov, P. A. Ryabochkina, V. Yu. Proydakova, V. V. Voronov, P. P. Fedorov, M. V. Chernov, Chinese Optics Letters **16**(9), 091901(2018).
- [7] Junlin Yuan, Xiaoyan Zeng, Jingtai Zhao, Zhijun Zhang, Haohong Chen, Xinxin Yang, Journal of Physics D Applied Physics **41**, 105406 (2008).
- [8] Lin Lin, Hui Lin, Zhezhe Wang, Jixing Chen, Ruijie Huang, Xin Rao, Zhuohong Feng, Zhiqiang Zheng, Optical Materials **36**, 1065 (2014).
- [9] Lei Zhao, Deyin Wang, Yuhua Wang, Ye Tao, Journal of the American Ceramic Society **97**, 3913 (2014).
- [10] Jumpei Ueda, Tanabe Setsuhisa, Journal of Applied Physics **106**, 043101 (2009).
- [11] Dan Zhao, Faxue Ma, Zhiqianhg Wu, Lei Zhang, Wei Wei, Materials Chemistry & Physics **182**, 231 (2016).
- [12] Xiaoyun Mi, Jiacheng Sun, Peng Zhou, Hongyan Zhou, Di Song, Journal of Materials Chemistry C **3**, 4471 (2015).
- [13] K. Niu, R. Sun, Q. Chen, B. Man, H. Zhang, Photonics Research **6**(2) 72 (2018).
- [14] J. Cheng, J. Zhang, H. Zhang, M. Sardar, X. Bian, Z. Shen, X. Ni, J. Lu, Chinese Optics Letters **15**(12) 121602 (2017).
- [15] Zhipeng Lian, Jianfeng Sun, Zhaohui Ma, Journal of Crystal Growth **401**, 334 (2014).
- [16] H. Lu, Z. Wang, Z. Huang, J. Tao, H. Xiong, W. Qiu, H. Guan, H. Dong, J. Dong, W. Zhu, J. Yu, Y. Zhong, Y. Luo, J. Zhang, Z. Chen, Photonics Research **6**(12) 1137 (2018).
- [17] Yubin Zeng, Zhengquan Li, Yingfang Liang, Xiaoqin Gan, Mengmeng Zheng, Inorganic Chemistry **52**, 9590 (2013).
- [18] W. B. Dai, J. L. Wang, Y. Y. Ma, Q. Y. Zhang, ECS J. Solid State Science & Technology **3**(12), R251 (2014).
- [19] Yuhua Wang, Lechun Xie, Huijuan Zhang, Journal of Applied Physics **105**, 663 (2009).
- [20] Chenxia Li, Jian Dai, Degang Deng, Optik-International Journal for Light and Electron Optics **127**, 2715 (2016).
- [21] Songsong An, Jia Zhang, Ceramics International **42**, 3437 (2016).
- [22] Chenxia Li, Jian Dai, Jun Huang, Ceramics International **42**, 6891 (2016).
- [23] Yixuan Lu, Chenxia Li, Degang Deng, Fengping Ruan, Le Wang, Shiqing Xu, Journal of Luminescence **196**, 25 (2018).
- [24] Z. Li, H. Wang, B. Yu, X. Ding, Y. Tang, Chinese Optics Letters **15**(4), 042301(2017).
- [25] Y. D. Peng, Z. J. Zhang, X. Q. Wang, S. D. Liu, A. H. Yang, X. S. Wang, Optical and Quantum Electronics **50**(8), 311 (2018).

*Corresponding author: lichenxia@cjlu.edu.cn
dengdegang@cjlu.edu.cn